

Effects of Preprocessing on Multi-Direction Properties of Aluminum Alloy Cold-Spray Deposits

M. R. Rokni¹ · A. T. Nardi² · V. K. Champagne³ · S. R. Nutt¹

Submitted: 16 January 2018 / in revised form: 24 April 2018 / Published online: 10 May 2018
© ASM International 2018

Abstract The effects of powder preprocessing (degassing at 400 °C for 6 h) on microstructure and mechanical properties of 5056 aluminum deposits produced by high-pressure cold spray were investigated. To investigate directionality of the mechanical properties, microtensile coupons were excised from different directions of the deposit, i.e., longitudinal, short transverse, long transverse, and diagonal and then tested. The results were compared to properties of wrought 5056 and the coating deposited with as-received 5056 Al powder and correlated with the observed microstructures. Preprocessing softened the particles and eliminated the pores within them, resulting in more extensive and uniform deformation upon impact with the substrate and with underlying deposited material. Microstructural characterization and finite element simulation indicated that upon particle impact, the peripheral regions experienced more extensive deformation and higher temperatures than the central contact zone. This led to more recrystallization and stronger bonding at peripheral regions relative to the contact zone area and yielded superior properties in the longitudinal direction compared with the short transverse direction. Fractography revealed that crack propagation takes place along the particle-particle interfaces in the transverse directions (caused by

insufficient bonding and recrystallization), whereas through the deposited particles, fracture is dominant in the longitudinal direction.

Keywords aluminum · high-pressure cold spray · mechanical properties · microstructure · powder preprocessing

Introduction

Cold-spray (CS) systems can be classified as either high pressure (HPCS) or low pressure (LPCS), based on the pressure level of the working gas. HPCS has become popular because they overcome major shortcomings of more conventional LPCS. One of the most important advantages of HPCS is the reduction in porosity levels in the deposit, owing to the much greater particle velocities and temperatures achieved. As a result, highly consolidated layers with superior mechanical properties can be produced (Ref 1-8).

While particles experience large strains during HPCS, the strains are non-homogenous (Ref 1, 2, 9, 10). The large strains lead to large flattening ratios ($R_f = \frac{D}{d_p}$) for the impacting powder particles, resulting in much greater diameters in the flattened particles (D) than those of the original particles (d_p). This characteristic produces distinct microstructures in the longitudinal (perpendicular to impact) and short transverse (parallel to impact) directions, which can result in anisotropic properties, e.g., strength and ductility. Thus, this study attempts to determine anisotropy in microstructure and mechanical properties of HPCS deposits.

✉ M. R. Rokni
rokni@usc.edu; mreza.rokni@gmail.com

¹ M.C. Gill Composites Center, Department of Chemical Engineering and Materials Science, University of Southern California, Los Angeles, CA, USA

² United Technologies Research Center, East Hartford, CT, USA

³ U.S. Army Research Laboratory, Weapons and Materials Research Directorate, Aberdeen Proving Ground, MD, USA

Because of the heterogeneous deformation that occurs during HPCS, deposits generally exhibit ultra-fine grains (UFG) or pancake grains at prior particle boundaries (PPBs), with larger grains (micron size) and high dislocation densities in particle interiors (Ref 2, 4, 10–16). Microscopically, this non-uniform deformation causes local variations in mechanical properties in the CS deposits (Ref 2, 3, 9, 16). At the macroscopic level, CS deposits achieve strength levels equal to wrought alloys, but with lower ductility due to porosity at some PPBs (Ref 2–6, 17–19). Effort has been devoted to improving the uniformity of CS materials by post-CS heat treatment, i.e., aging and annealing, altering the microstructure of the deposits to achieve superior combinations of ductility and strength (Ref 3, 6, 18–22). However, this approach can be difficult or unacceptable from a practical perspective because of component size, base material, or specific production process.

Besides, gas-atomized powders typically exhibit a cellular/dendritic microstructure with composition variations between grain boundaries (GBs) and grain interiors, particularly GB solute segregation (Ref 11, 13, 14, 17, 23–26), mainly due to the nature gas atomization process (Ref 13, 23, 26). These composition variations, especially for precipitation-strengthened aluminum (Al) alloys, lead to lack of strengthening precipitates in the matrix and a brittle intermetallic network on the GBs. Such a microstructure will result in inferior strength and ductility in resultant CS coatings. However, eliminating the intermetallic network through powder preprocessing could not only resolve this issue, but also improve particle formability during CS the deposition process (Ref 26–28). Because of these reasons, we have attempted to preprocess the gas-atomized powder and to homogenize the microstructure and remove GB solute segregation. In so doing, we expect to achieve strength and ductility levels equivalent to wrought alloys.

The 5xxx series Al alloys are solution hardenable, the primary solute being magnesium (Mg). Among these alloys, 5056 Al features attractive ballistic and corrosion properties, good weldability, and cost. In this study, we investigate the microstructure and mechanical property relationships in CS 5056 Al deposits produced with preprocessed gas-atomized powder. Directionality in mechanical properties was evaluated by microtensile testing, and variations were correlated with microstructural analysis. Understanding more clearly the relationships between the preprocessed powder microstructure and the CS deposit microstructures, as well as property directionality, is critical to efforts to control product microstructure and produce CS deposits with optimal properties and performance.

Experimental Procedure

Powder Processing

The gas-atomized 5056 Al powder (Valimet, Stockton, CA, USA) was heat-treated prior to cold spraying. The powder was processed at 400 °C in nitrogen for 6 h (Table 1) and then cooled to room temperature while continuing to flow nitrogen. The powder heat treatments were performed using a fluidized bed heat treatment process, which maintains relative motion between powder particles while transporting away gases and moisture through the fluidizing gas before they can react further with other powders within the bed. This method of heat treatment negates the problems associated with sintering of the powders at these temperatures. The details of the furnace and the applied procedure for heat treatment can be found in Ref 27.

Cold-Spray Processing

5056 Al coatings were produced using the as-received and preprocessed 5056 Al powders and spraying onto a wrought 5056 aluminum alloy substrate. Helium was used as the process gas to achieve high-impact velocities. The deposits were produced using a HPCS system (VRC Gen III, VRC Metal Systems, Rapid City, SD, USA), and helium pressure and temperature were maintained at 2.8 MPa and 400 °C at the heater exit. Deposition was performed using a nozzle standoff distance of 25 mm, 90° deposition angle, medium powder feed rate (12 g min⁻¹), and a nozzle traveling speed of 600 mm s⁻¹. A total deposition thickness of ~ 15 mm was achieved.

Microstructural Characterization

The microstructure of the preprocessed powder was evaluated by scanning electron microscopy (SEM), electron backscattered diffraction (EBSD), and energy-dispersive x-ray spectroscopy (EDS). SEM and EBSD samples were prepared by ion polishing after mounting powders in epoxy (JEOL SM-09010, Tokyo, Japan).

The microstructure of the 5056 deposits was also characterized by light microscopy (LM), SEM, and EBSD. For the microstructural observations of the deposited materials, sections were excised by electrical discharge machining

Table 1 Time and temperature for the applied preprocessing heat treatment

| Heat treatment | Temperature, °C | Time, h |
|----------------|-----------------|---------|
| Degassing | 400 | 6 |

(EDM) from different directions and then mounted in epoxy resin prior to ion polishing.

Mechanical Properties

The effects of powder preprocessing on mechanical properties of 5056 aluminum deposits were evaluated using tensile testing of miniature samples. The results were compared to longitudinal properties of wrought 5056 and the coating deposited with as-received 5056 Al powder. The directionality of mechanical properties of deposits (produced from preprocessed 5056 powder) was also evaluated using the microtensile testing. As shown in Fig. 1, coupons were cut along longitudinal, short transverse, long transverse, and diagonal (45° to the deposition direction) directions. Five samples were tested for each direction using the configuration shown in Fig. 2. To avoid damage and to obtain dimensionally accurate samples, EDM was employed to cut the miniature tensile coupons. As shown in Fig. 2, the gauge lengths of the tensile samples were 1 mm, and cross-sectional areas were approximately $1 \times 0.5 \text{ mm}^2$. Microtensile testing was performed at room temperature using a microtensile stage (Microtest, Deben Ltd., East Grinstead, UK) at a crosshead speed of $3.3 \times 10^{-3} \text{ mm/min}$. Samples were tested to failure, and the load-displacement curves were converted to engineering stress versus engineering strain. The ultimate tensile strength (UTS) and the elongation to failure were determined from the stress-strain curves.

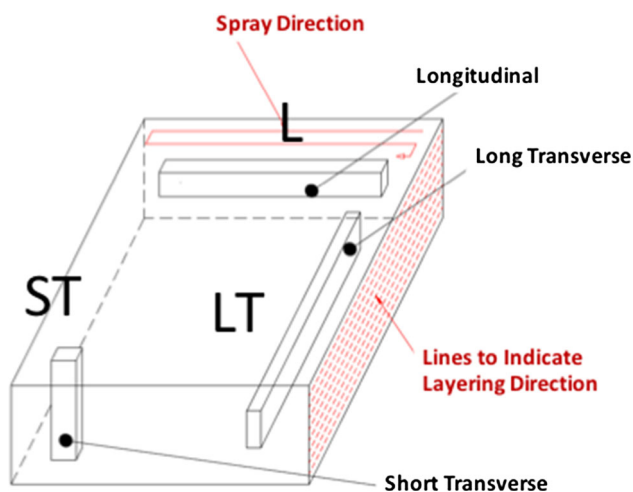


Fig. 1 Schematic showing the spray direction and the directions from which microtensile samples were cut. The diagonal direction is not shown in this image

Results and Discussion

Microstructural Characterization

As-received Powder

Figure 3 shows the morphology and surface grain structure of the preprocessed gas-atomized powder particles. Most of the particles are spherical with an average diameter of $33.7 \pm 8.5 \mu\text{m}$. Microsatellite particles (less than $5 \mu\text{m}$ diameter) are also attached to the surface of the larger particles. Figure 3(b) shows a typical powder particle $\sim 30 \mu\text{m}$ in diameter. There is a $\sim 1\text{--}3\text{-}\mu\text{m}$ external grain structure on the particle surface, shown enlarged in Fig. 3(c).

As shown in Fig. 3(c), EDS point analysis was performed on the particle surface to determine composition variations between GBs and grain interiors. The results, tabulated in Table 2, show no significant Mg segregation across these two regions. This finding indicates that the preprocessing of the 5056 powder yielded a more uniform dispersion of solute elements in the microstructure of the powder particles. EDS mapping of particle cross sections supported this finding. Figure 4 shows that Mg, the primary solute in 5056 Al, is uniformly distributed within the preprocessed powder particles, and there is no sign of solute segregation. This observation differs from what has been widely reported in as-received gas-atomized powders (Ref 11, 13, 14, 17, 23–26).

Figure 5 shows the ion-polished microstructures of the feedstock powder cross section in as-received and degassed conditions. The internal microstructure of the as-received powder in Fig. 5(a) and (b) is characterized by a cellular-like dendritic structure, similar to that found on the surface

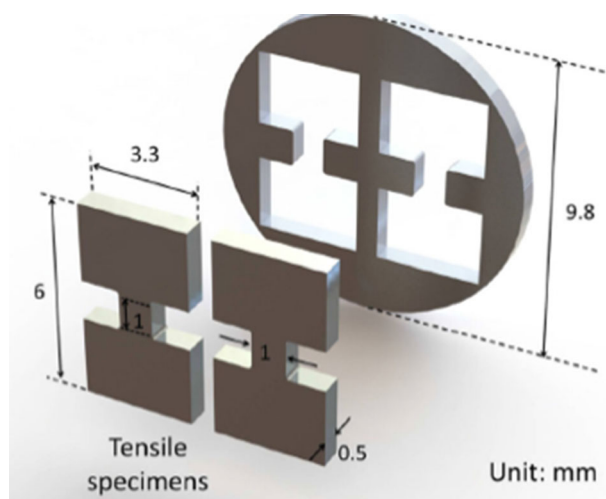


Fig. 2 Specimen geometry used for microtensile testing. All dimensions are in mm

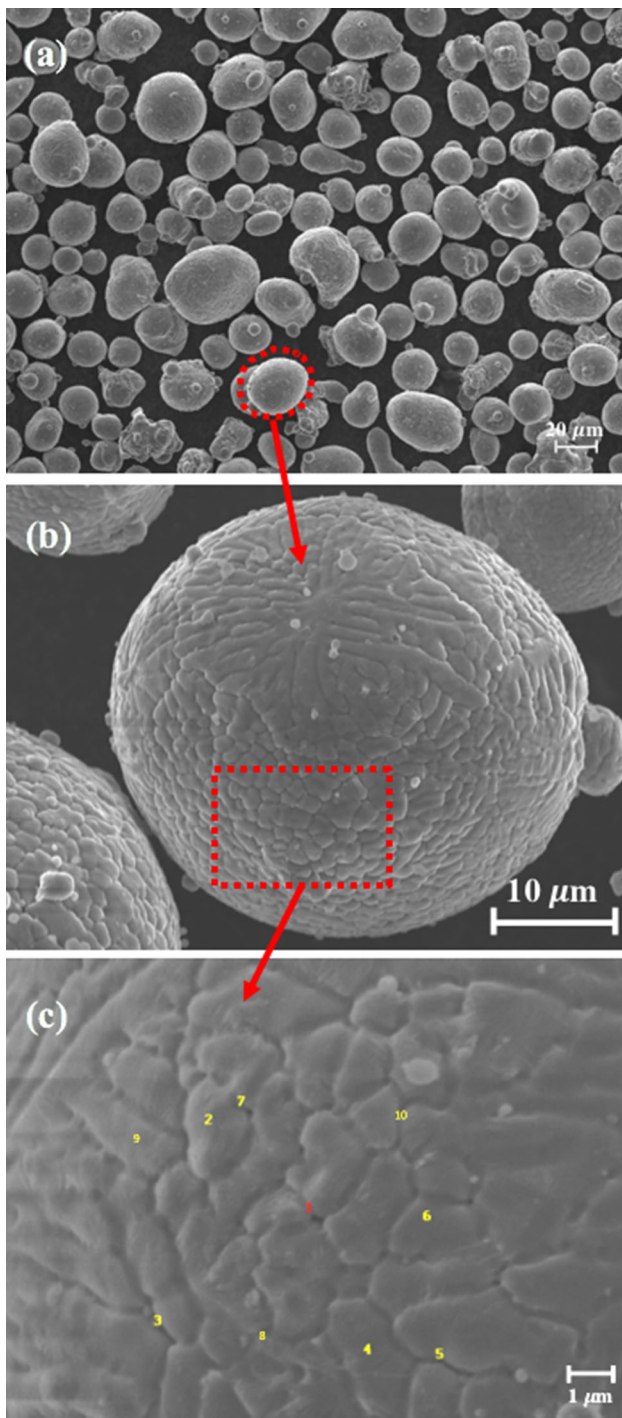


Fig. 3 SEM micrographs from preprocessed gas-atomized 5056 Al powder showing (a) powder morphology, (b) surface grain structure, and (c) EDS point analysis on the particle surface

of the particles. This observation agrees with what has been reported for other gas-atomized Al powders (Ref 11, 13, 14, 17, 24). However, as shown in Fig. 5(c) and (d), particles contain larger grains in the degassed condition, which is attributed to grain growth during preprocessing. The difference in the grain structures of the degassed

Table 2 EDS point analysis results from the preprocessed 5056 powder particle surface

| Point, wt. % | O | Mg | Al |
|--------------|------|------|-------|
| 1 | 2.47 | 9.15 | 88.38 |
| 2 | 2.45 | 9.00 | 88.55 |
| 3 | 2.61 | 9.30 | 88.09 |
| 4 | 2.50 | 8.90 | 88.60 |
| 5 | 2.81 | 9.30 | 87.89 |
| 6 | 2.60 | 9.18 | 88.23 |
| 7 | 2.60 | 8.78 | 88.62 |
| 8 | 2.75 | 8.72 | 88.53 |
| 9 | 2.12 | 9.29 | 88.59 |
| 10 | 2.33 | 8.78 | 88.99 |
| STDEV.P | 0.19 | 0.22 | 0.30 |
| AVE | 2.51 | 9.04 | 88.45 |

particles in Fig. 5(c) and (d) is related to inadequate stirring during preprocessing, which causes the particles to experience different levels of grain growth during the degassing process.

Cold-Sprayed Deposition

Figure 6 shows an LM image and a pattern quality EBSD image from the short transverse direction (cross section) of the 5056 deposit. The deposit shows no porosity and apparent bonding between powder particles. Most particles have flattened (pancaked) during cold spraying (yellow arrows), and only a few exhibit light deformation and microstructure similar to the feedstock powder (white arrows). Similar observations have been reported for other cold-sprayed deposits (Ref 2-4, 11-14). The significant change in particle morphology during cold spraying is the result of severe plastic deformation (SPD) during impact with the underlying substrate and impact from subsequently arriving powder particles.

Figure 7 shows an Euler angle EBSD map obtained from the short transverse direction. The black dashed line indicates a prior particle boundary (PPB), where grain structures are different from particle interiors. The depositing particles experience recrystallization in peripheral and central contact regions. However, as shown in Fig. 7, the extent of recrystallization is greater in the peripheral region (red square, finer grains) than at the central contact zone (white rectangle). This observation indicates that peripheral regions undergo more deformation and greater adiabatic shear instabilities (ASI) and thus experience higher temperatures during HPCS (Ref 28-33). This is also the main reason that voids are consistently reported at the impact zone of particles, but usually tend to

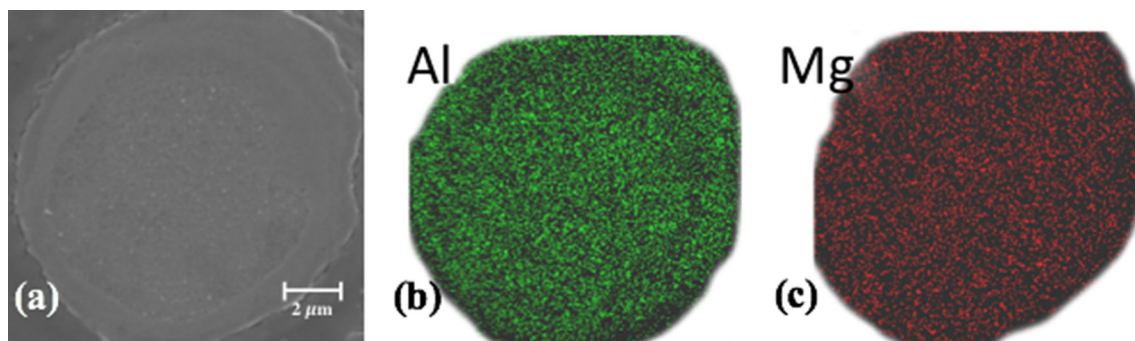


Fig. 4 EDS maps of the preprocessed gas-atomized 5056 powder particles

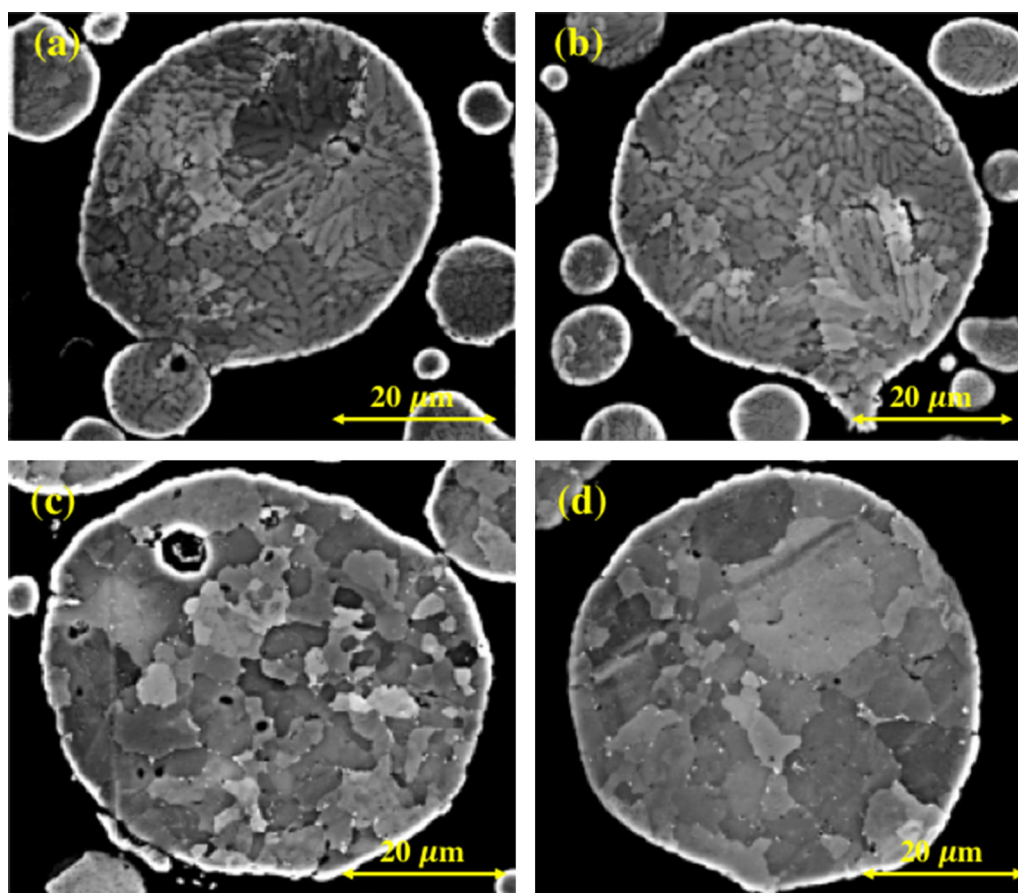


Fig. 5 EBSD maps of the preprocessed 5056 Al powder particles with different sizes

disappear at the peripheral regions (although not always) (Ref 31).

The presence of lighter deformation and lower temperatures, i.e., less recrystallizations, in the central zone was further supported by finite element analysis (FEA) of a 5056Al particle impact onto 5056Al substrate during cold spraying. The black arrows in Fig. 8(a) and (b) indicate the center of the impact zone in the deposited particle and the substrate, which reveals that this area does not experience

intense deformation and/or high temperature. This means when strains and temperatures are mapped over the particle-substrate interface, it is found that they are much greater in the peripheral regions (i.e., within the shear jets) than at the impact zone of the particle (Ref 30, 32). The effects of non-uniform recrystallization on mechanical property directionality and related bonding for the 5056 deposit were evaluated by microtensile testing, described next.

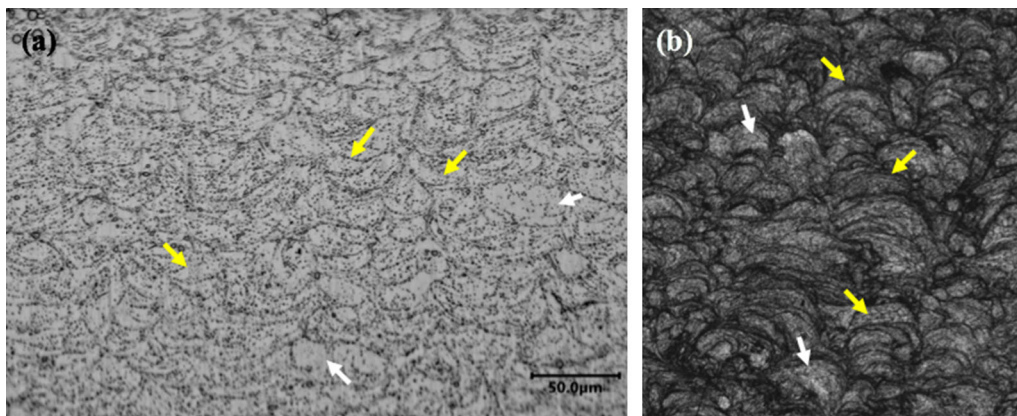


Fig. 6 (a) LM and (b) pattern quality EBSD images from the cross section (short transverse direction) of the CS 5056 Al deposit. Yellow and white arrows show severely and lightly deformed particles, respectively (Color figure online)

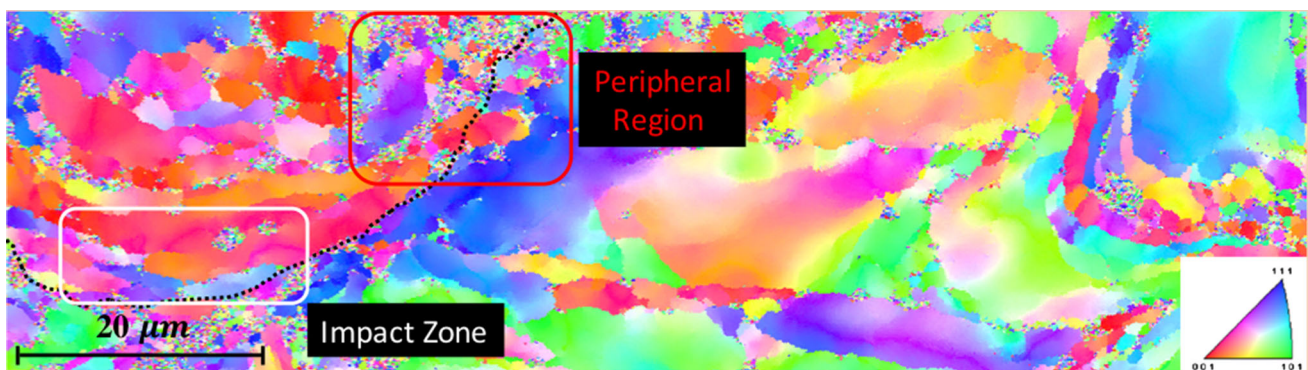


Fig. 7 EBSD map indicating the extents of recrystallization at the peripheral and impact regions between two particles

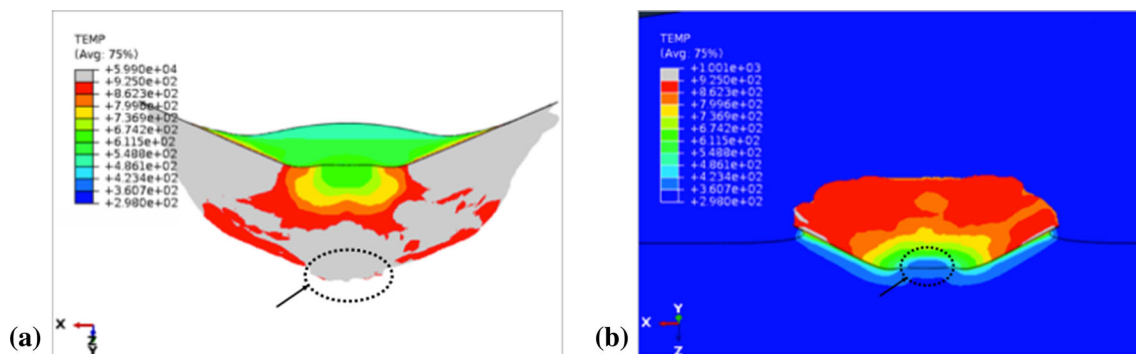


Fig. 8 FEA simulation of particle impact during CS process showing lack of bonding at central area of the impact zone with black arrow in the (a) particle and (b) substrate ($d_p = 25 \mu\text{m}$, $T_{p0} = 509^\circ\text{K}$, $V_0 = 980 \text{ m/s}$ for depositing 5056Al on 5056Al substrate)

Tensile Properties and Fractography

Figure 9 shows the UTS and elongation to fracture for the 5056 Al microtensile coupons in all four directions. The longitudinal properties for wrought 5056 Al and the 5056 Al coating deposited with as-received powder are included here for comparison. The preprocessed 5056 coating shows UTS values in longitudinal (*L*), diagonal, and long transverse directions ($\sim 413 \text{ MPa}$) equivalent to wrought 5056

Al, and greater than that of the coating deposited with as-received powder ($\sim 398 \text{ MPa}$), indicating that the UTS improves with preprocessing. However, the UTS decreased by 20% (to $331 \text{ MPa} \pm 14$) for the short transverse (*ST*) direction.

Ductility of the preprocessed coating was equivalent to wrought alloy ductility ($5.9\% \pm 0.2$), while it was greater by almost 50% from that of the coating deposited with the as-received powder. Preprocessing softened the particles

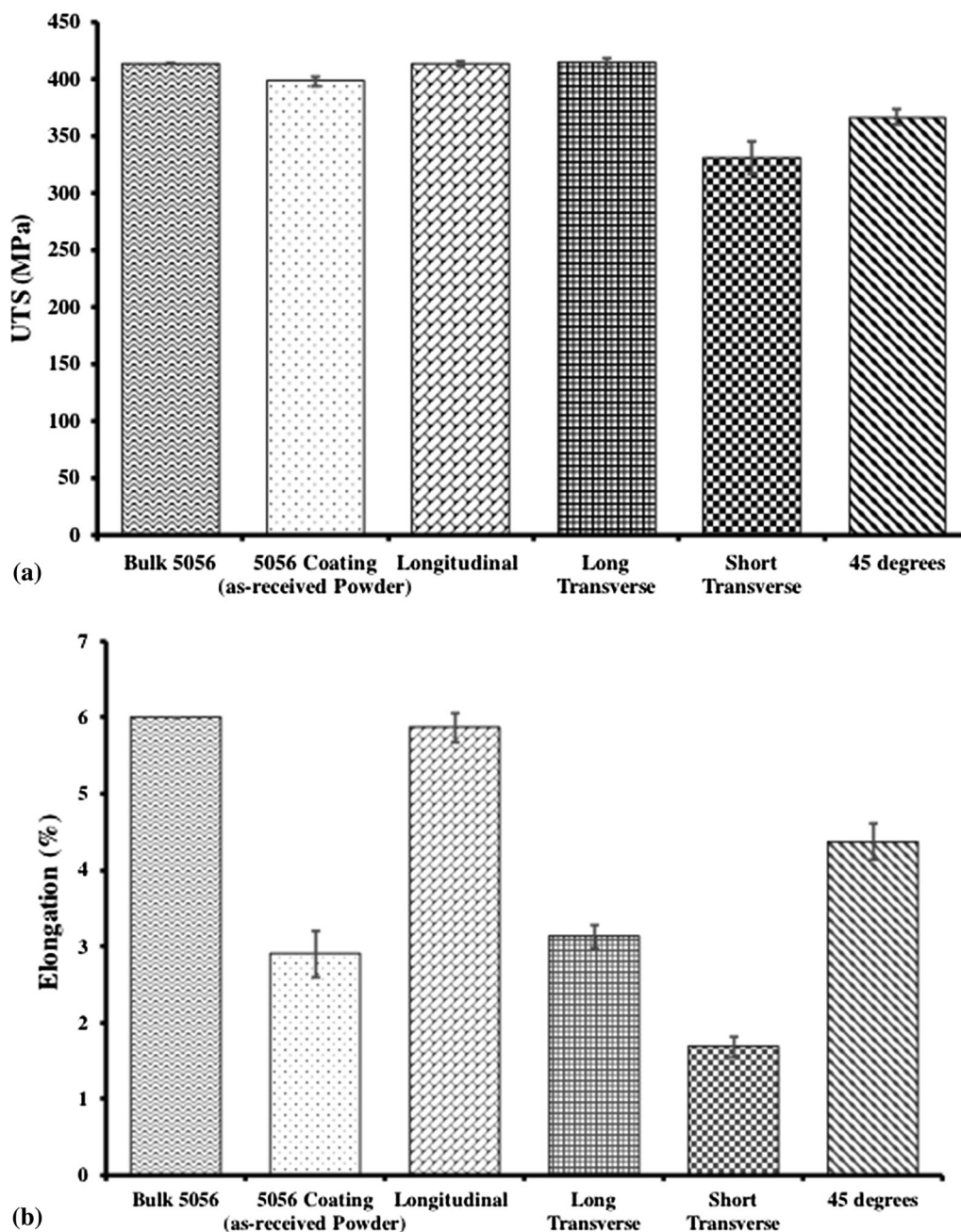


Fig. 9 The (a) UTS and (b) elongation to fracture of microtensile specimens of the CS 5056 Al deposit in different directions. The UTS and elongation of bulk 5056 Al have also been added to the graphs to comparison

and eliminated the pores within them, resulting in more extensive and uniform deformation upon impact with the substrate and with underlying deposited material, which consequently lead to the improvements in UTS and ductility. Ductility in the *ST* direction was the lowest among all directions tested ($1.7\% \pm 0.1$), while, as expected, the strength and ductility in the diagonal direction was an average of all the other directions.

To more clearly understand the difference in mechanical properties of *ST* and *L* directions and the primary

deformation mechanisms, fracture surfaces of the tensile samples were analyzed. These directions were chosen for analysis because of the difference in ductility (5.9% in *L* versus 1.7% in *ST* direction), which could illuminate bonding conditions at PPBs in the CS samples.

The fracture surfaces of *ST* and *L* directions are shown in Fig. 10(a) and (b). As indicated by yellow arrows in Fig. 10(a), fracture separation in the *ST* direction occurred primarily at PPBs, and entire particles detached during fracture. In contrast, fractography of *L* samples showed that

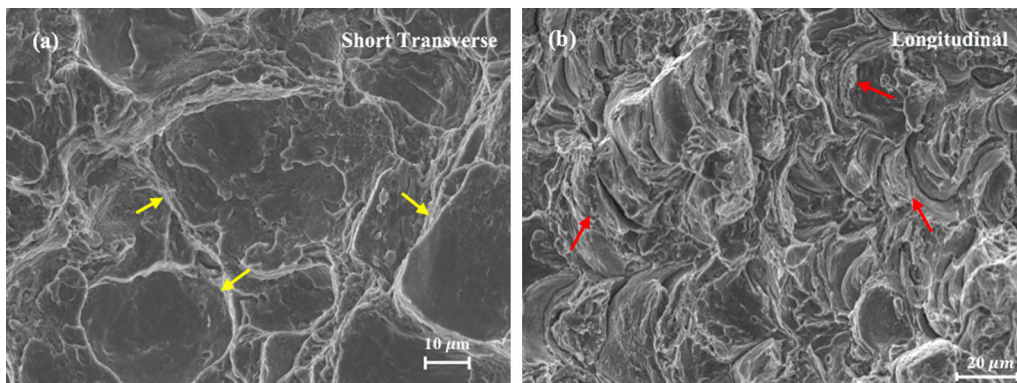


Fig. 10 Fracture surfaces of microtensile specimens of the CS 5056 Al deposit from short transverse and longitudinal directions. The yellow arrows show the location of fracture separation in each direction (Color figure online)

the fracture propagated both through the particle interfaces and through particle interiors, indicated by red arrows in Fig. 10(b). These observations point out that crack propagation takes place along the interface and through the deposited particles in the *ST* and *L* directions, respectively.

Recall that peripheral regions of deposited particles experience more intense deformation and greater ASI during particle impact (Fig. 7 and 8), which result in disruption of the surface oxide and exposure of fresh alloy in these regions (Ref 29–34). In addition, thermal softening due to SPD and ASI can enhance interlocking of adjacent particles, producing intimate contact. SPD and ASI lead to stronger bonding between the particles in the *L* direction and cause fracture to propagate through particle interiors and PPBs. However, we speculate that less intense SPD and ASI at the central contact zone leads to the presence of oxide remnants in this area. This phenomenon along with high hydrostatic pressures in the central contact zone during cold spraying gives rise to weaker bonding in these regions, which translates to inferior mechanical properties, i.e., lower UTS and ductility, in the *ST* direction relative to the *L* direction.

Summary

We have reported the relationships between the preprocessed powder and CS deposit microstructure and property directionality. Preprocessing leads to more homogenous distribution of Mg solute in the Al matrix removing GB solute segregation. Preprocessing also softens the powder particles and results in greater ASI during HPCS. These phenomena give rise to more intense SPD and higher temperatures at peripheral regions of deposited particles, disrupting the oxide layer and causing more extensive recrystallization in these regions compared to impact areas. Exposing fresh alloy and catalyzing recrystallization in peripheral regions appeared to enhance bonding between

the deposited particles in the longitudinal direction, which yielded values of UTS and ductility equivalent to those of wrought Al. The presence of some oxide remnants and insufficient recrystallization in the short transverse direction resulted in weaker bonding and reduced ductility values in this direction. Similar phenomena caused intergranular fracture in the longitudinal direction, whereas transgranular fracture was observed in the short transverse direction.

Overall, thermal processing of feedstock powders prior to deposition, i.e., pre-CS processing, if properly done, can yield measurable benefits. First, it can lead to uniform distribution of alloying elements in the powder particles. Second, it can soften the particles, consequently giving rise to more intensive particle deformation during cold spraying. These features can promote greater bonding upon impact with the substrate (adhesion) or with underlying deposits (cohesion), enhancing the UTS and ductility in the resultant deposit. These advances can have beneficial implications for CS repair and refurbishment of sensitive parts and components, leading to increased life spans in service applications.

Acknowledgments The authors acknowledge financial support from the Army Research Lab (ARL) under Contract No. W911NF-11-2-0014. The authors also thank Mr. R.H. Hrabec and Dr. C.W. Widener from VRC Metal Systems for helpful discussions and assistance with the interpretation of results, and UTRC for coordinating the deposition of materials used for analysis.

References

1. V.K. Champagne, *The Cold Spray Materials Deposition Process: Fundamentals and Applications*, Woodhead Publishing Limited, Cambridge, 2007
2. M.R. Rokni, C.A. Widener, G.A. Crawford, and M.K. West, An Investigation into Microstructure and Mechanical Properties of Cold Sprayed 7075 Al Deposition, *Mater. Sci. Eng. A*, 2015, **625**, p 19–27

3. P. Vo, E. Irissou, J.G. Legoux, and S. Yue, Mechanical and Microstructural Characterization of Cold-Sprayed Ti-6Al-4 V After Heat Treatment, *J. Therm. Spray Technol.*, 2013, **22**, p 954-964
4. M.R. Rokni, C.A. Widener, V.K. Champagne, and G.A. Crawford, Microstructure and Mechanical Properties of Cold Sprayed 7075 Deposition During Non-isothermal Annealing, *Surf. Coat. Technol.*, 2015, **276**, p 305-315
5. V.K. Champagne, III, M.K. West, M.R. Rokni, T. Curtis, V.R. Champagne, Jr., and B. McNally, Joining of Cast ZE41A Mg to Wrought 6061 Al by the Cold Spray Process and Friction Stir Welding, *J. Therm. Spray Technol.*, 2016, **25**, p 143-159
6. P.D. Eason, J.A. Fewkes, S.C. Kennett, T.J. Eden, K. Tello, M.J. Kaufman, and M. Tiryakioğlu, On the Characterization of Bulk Copper Produced by Cold Gas Dynamic Spray Processing in as Fabricated and Annealed Conditions, *Mater. Sci. Eng. A*, 2011, **528**, p 8174-8178
7. H.J. Kim, C.-H. Lee, and S.-Y. Hwang, Fabrication of WC-Co Coatings by Cold Spray Deposition, *Surf. Coat. Technol.*, 2005, **191**, p 335-340
8. K. Spencer and M.-X. Zhang, Heat Treatment of Cold Spray Coatings to form Protective Intermetallic Layers, *Scr. Mater.*, 2009, **61**, p 44-47
9. Y. Zou, D. Goldbaum, J.A. Szpunar, and S. Yue, Microstructure and Nanohardness of Cold-Sprayed Coatings: Electron Backscattered Diffraction and Nanoindentation Studies, *Scr. Mater.*, 2010, **62**, p 395-398
10. M.R. Rokni, C.A. Widener, A.T. Nardi, and V.K. Champagne, Nano Crystalline High Energy Milled 5083 Al Powder Deposited Using Cold Spray, *Appl. Surf. Sci.*, 2014, **305**, p 797-804
11. M.R. Rokni, C.A. Widener, and G.A. Crawford, *Surf. Coat. Technol.*, 2014, **251**, p 254-263
12. T. Schmidt, H. Assadi, F. Gärtner, H. Richter, T. Stoltenhoff, H. Kreye, and T. Klassen, From Particle Acceleration to Impact and Bonding in Cold Spraying, *J. Therm. Spray Technol.*, 2009, **18**, p 794-808
13. M.R. Rokni, C.A. Widener, S.P. Ahrenkiel, B.K. Jasthi, and V.K. Champagne, Annealing Behaviour of 6061 Aluminium Deposited by High Pressure Cold Spray, *Surf. Eng.*, 2014, **30**, p 361-368
14. M.R. Rokni, C.A. Widener, and V.K. Champagne, Microstructural Evolution of 6061 Aluminum Gas-Atomized Powder and High-Pressure Cold-Sprayed Deposition, *J. Therm. Spray Technol.*, 2014, **23**, p 514-524
15. L. Ajdelsztajn, B. Jodoin, G.E. Kim, and J.M. Schoenung, Cold Spray Deposition of Nanocrystalline Aluminum Alloys, *Metal. Mater. Trans. A*, 2005, **6**, p 657-666
16. D. Goldbaum, R.R. Chromik, S. Yue, E. Irissou, and J.-G. Legoux, Mechanical Property Mapping of Cold Sprayed Ti Splats and Coatings, *J. Therm. Spray Technol.*, 2011, **20**, p 486-496
17. M.R. Rokni, S.R. Nutt, C.A. Widener, V.K. Champagne, and R.H. Hrabec, Review of Relationship Between Particle Deformation, Coating Microstructure, and Properties in High-Pressure Cold Spray, *J. Therm. Spray Technol.*, 2017, **26**, p 1308-1355
18. M.R. Rokni, C.A. Widener, V.K. Champagne, G.A. Crawford, and S.R. Nutt, The Effects of Heat Treatment on 7075 Al Cold Spray Deposits, *Surf. Coat. Technol.*, 2017, **310**, p 278-285
19. M.R. Rokni, C.A. Widener, O.C. Ozdemir, and G.A. Crawford, Microstructure and Mechanical Properties of Cold Sprayed 6061 Al in As-Sprayed and Heat Treated Condition, *Surf. Coat. Technol.*, 2017, **309**, p 641-650
20. F. Gärtner, T. Stoltenhoff, J. Voyer, H. Kreye, S. Riekehr, and M. Koçak, Mechanical Properties of Cold-Sprayed and Thermally Sprayed Copper Coatings, *Surf. Coat. Technol.*, 2006, **200**, p 6770-6782
21. X.-M. Meng, J.-B. Zhang, W. Han, J. Zhao, and Y.-L. Liang, Influence of Annealing Treatment on the Microstructure and Mechanical Performance of Cold Sprayed 304 Stainless Steel Coating, *Appl. Surf. Sci.*, 2011, **258**, p 700-704
22. B. AL-Mangour, P. Vo, R. Mongrain, E. Irissou, and S. Yue, Effect of Heat Treatment on the Microstructure and Mechanical Properties of Stainless Steel 316L Coatings Produced by Cold Spray for Biomedical Applications, *J. Therm. Spray Technol.*, 2014, **23**, p 641-652
23. L.N. Brewer, J.F. Schiel, E.S.K. Menon, and D.J. Woo, The Connections Between Powder Variability and Coating Microstructures for Cold Spray Deposition of Austenitic Stainless Steel, *Surf. Coat. Technol.*, 2018, **334**, p 50-60
24. L. Ajdelsztajn, A. Zúñiga, B. Jodoin, and E.J. Lavernia, Cold Gas Dynamic Spraying of a High Temperature Al Alloy, *Surf. Coat. Technol.*, 2006, **201**, p 2109-2116
25. Y.Y. Zhang, X.K. Wu, H. Cui, and J.S. Zhang, Cold-Spray Processing of a High Density Nanocrystalline Aluminum Alloy 2009 Coating Using a Mixture of As-Atomized and As-Cryomilled Powders, *J. Therm. Spray Technol.*, 2011, **20**, p 1125-1132
26. G. Berube, M. Yandouzi, A. Zuniga, L. Ajdelsztajn, J. Villafuerte, and B. Jodoin, Phase Stability of Al-5Fe-V-Si Coatings Produced by Cold Gas Dynamic Spray Process Using Rapidly Solidified Feedstock Materials, *J. Therm. Spray Technol.*, 2012, **21**, p 240-254
27. W.A. Story and L.N. Brewer, Heat Treatment of Gas-Atomized Powders for Cold Spray Deposition, *Metall. Mater. Trans. A*, 2018, **49**, p 446-449
28. Y. SheAaron T. Nardi, and L. Binek, System for Powder Heat Treatment and Classification via Fluidized Bed, US2017017359, Year of Priority (issued): 2015 (2017)
29. S. Yin, X.F. Wang, W.Y. Li, H.L. Liao, and H.E. Jie, Deformation Behavior of the Oxide Film on the Surface of Cold Sprayed Powder Particle, *Appl. Surf. Sci.*, 2012, **259**, p 294-300
30. Q. Wang, D. Qiu, Y. Xiong, N. Birbilis, and M.-X. Zhang, High Resolution Microstructure Characterization of the Interface Between Cold Sprayed Al Coating and Mg Alloy Substrate, *Appl. Surf. Sci.*, 2014, **289**, p 366-369
31. H. Assadi, F. Gärtner, T. Stoltenhoff, and H. Kreye, Bonding Mechanism in Cold Gas Spraying, *Acta Mater.*, 2003, **51**, p 4379-4394
32. P.C. King, G. Bae, S. Zahiri, M. Jahedi, and C. Lee, An Experimental and Finite Element Study of Cold Spray Copper Impact onto Two Aluminum Substrates, *J. Therm. Spray Technol.*, 2010, **19**, p 620-634
33. Y. Xiong, X. Xiong, S. Yoon, G. Bae, and C. Lee, Dependence of Bonding Mechanisms of Cold Sprayed Coatings on Strain-Rate-Induced Non-equilibrium Phase Transformation, *J. Therm. Spray Technol.*, 2011, **20**, p 860-865
34. P.C. King, S.H. Zahiri, and M. Jahedi, Microstructural Refinement Within a Cold-Sprayed Copper Particle, *Metal. Mater. Trans A*, 2009, **40**, p 2115-2123